CMS Physics Analysis Summary

Contact: cms-future-conveners@cern.ch 2017/05/07

ECFA 2016: Prospects for selected standard model measurements with the CMS experiment at the High-Luminosity LHC

The CMS Collaboration

Abstract

The prospects for selected standard model measurements at the High-Luminosity LHC presented at ECFA 2016 workshop are summarized. The extrapolations assume proton-proton collision data at a centre-of-mass energy of 14 TeV corresponding to an integrated luminosity of up to $3\,\text{ab}^{-1}$. The achievable precision for top quark mass measurements based on different analysis strategies is estimated. Searches for flavour-changing neutral currents in top quark decays are studied and expected limits are set, based on different scenarios for the extrapolation of systematic uncertainties to the High-Luminosity LHC run conditions. The feasibility of a dedicated track trigger for the $B_s \to \phi\phi$ decay studies is discussed.

1 Introduction

The High-Luminosity LHC (HL-LHC) [1] is the proposed upgrade of the LHC which has the goal of accumulating 3000 fb^{-1} of integrated luminosity in proton-proton (pp) collisions at a centre-of-mass energy ($\sqrt{s}$) of 14 TeV. For this, the number of additional interactions per bunch crossing (pileup) ranges from a nominal value of 140 up to 200, requiring upgraded detectors to maintain good physics performance. It is assumed that the CMS tracker will be extended up to $|\eta| = 3.8$ and will provide a selective readout of tracks with $p_{\text{T}} > 2\,\text{GeV}$ at 40 MHz that can be used for trigger purposes. The coverage of the resistive plate chambers of the muon system will also be extended up to $|\eta| = 2.4$ and muon tagging will be possible up to $|\eta| = 3$. The detector endcaps will consist of radiation tolerant high granularity silicon hadronic and electromagnetic calorimeters with 3D readout capabilities. A comprehensive description of the CMS detector upgrade for the HL-LHC can be found in Refs. [2, 3].

One of the physics goals of this upgrade is to perform precise standard model (SM) measurements that require high accuracy and a significant amount of data. This note contains three physics studies that were presented at the ECFA 2016 workshop [4]. Section 2 presents extrapolations for measurements of the top quark mass, based on results obtained mainly at $\sqrt{s} = 8\,\text{TeV}$, with particular focus on the projected evolution of systematic uncertainties. Section 3 presents a search for flavour changing neutral currents (FCNC) in top quark events using a fast simulation of the upgraded detector for different scenarios of systematic uncertainties. Section 4 is devoted to the discussion of a possible track-based trigger for $B \to \phi\phi$ decay studies that are done with the full detector simulation. The motivations for each of the measurements, requirements, and results are discussed separately in each section. Since the analyses use very different techniques and aim at distinct physics goals, each section contains its own introduction, requirements and results subsections. The conclusions are also given separately for each analysis at the end of the corresponding section and are summarized in Section 5.

2 Improvement of the top quark mass measurements

The top quark is the heaviest known elementary particle. Its mass (m_{t}) is a fundamental parameter of the SM, affecting not only predictions in quantum chromodynamics (QCD), but also having fundamental implications for the electroweak sector. The top quark contributes significantly to the quartic Higgs coupling and affects constraints on the stability of the electroweak vacuum [5, 6], as well as on models with cosmological implications [7, 8].

This Section discusses the potential improvements in the precision of m_{t} measurements that can be achieved by the upgraded CMS detector at the HL-LHC. The run conditions and detector configuration assumed are those following the phase II upgrade which is scheduled for 2023. The projections are based on extrapolated uncertainties with integrated luminosities of between 0.3 and 3 ab^{-1} at a collision energy of 14 TeV.

In 2013, the previous study of the HL-LHC capabilities for m_{t} [9] was based on the knowledge derived from the initial CMS mass measurements at 7 TeV. The measurements used an integrated luminosity of 5 fb^{-1} and the first versions of the CMS mass analyses. The studies presented here provide an update of these projections and are based on m_{t} measurements performed with 19.7 fb^{-1} of data at 8 TeV. With this larger dataset, the CMS experiment has achieved a precision of 0.49 GeV (0.28%) on m_{t} [10].

As in Ref. [9], the above numbers do not include possible ambiguities [11] with respect to the theoretical interpretation of the measured m_{t}. Most analyses presented here measure the

"Monte-Carlo mass" (m_t^{MC}), while m_t in a well-defined renormalisation scheme can be extracted from the top quark pair ($t\bar{t}$) cross section by comparing the measured value with beyond leading-order predictions. With an uncertainty of about 1.8 GeV for the top quark pole mass at next-to-next-to-leading order (NNLO) in QCD [12], this technique does not reach a precision competitive with the most precise measurements, but it does provide a more straightforward interpretation of the measured m_t.

The measurements using $t\bar{t}$ events are discussed first. These typically calibrate the jet-energy scale (JES) simultaneously with measuring m_t. Recent analysis techniques have been developed to use in-situ constraints from the data for more than two parameters [13] (referred-to as "3D fits" in the following). A global jet-energy scale factor can be determined simultaneously with a residual energy correction for b jets [14, 15]. These thechniques are limited by statistical uncertainties. The same applies to differential measurements of m_t as a function of kinematic observables [16] (shortened to "differential" in Table 1–4), which give insight into different aspects of the modeling of QCD interactions. The HL-LHC will ultimately offer the possibility to constrain the systematic uncertainties related to jet energy scale calibration and the modeling of QCD interactions to an unprecedented precision.

The prospects for the m_t determination from single-top quark enriched samples are also reported. Single-top quark production is mediated through electroweak interactions and m_t measurements from single-top quark events are not sensitive to the modeling of QCD interactions in the same way as those in $t\bar{t}$ events. Other alternative approaches, labelled as the "secondary vertex" and "J/ψ" methods in the following, avoid the reconstruction of jets or rely solely on lepton reconstruction. This approach strongly reduces the traditional uncertainties related to the JES calibration and QCD processes and reduces the dependence on pileup. These measurements typically have larger statistical uncertainties. We estimate how these methods may profit from the large integrated luminosities at the HL-LHC. The precision of the results obtained using these techniques are compared to the more standard $t\bar{t}$ measurements and to those derived from the measured cross sections.

2.1 Assumptions

At the HL-LHC severe pileup conditions, with up to 200 interactions per bunch crossing, are expected. Pileup mitigation techniques have been improved with the replacement of the charge hadron subtraction (CHS) algorithm by the pileup per particle identification algorithm (PUPPI) [17]. Using PUPPI, the effect of pileup on the measurements is expected to be kept under control. In particular, it is assumed that there is no significant decrease in the jet energy resolution and that the reconstruction of the top quark or $t\bar{t}$ system from the final-state objects is not affected. However, high lepton p_T thresholds at the trigger level and high purity selection requirements are expected to lead to a decrease of trigger and selection efficiencies for all analyses. The increase of the $t\bar{t}$ production cross section by more than a factor of 3 from 8 TeV to 14 TeV [18] compensates for a loss of about 30% in trigger and selection efficiencies. The expected statistical uncertainty is thus assumed to scale with the square root of the increased luminosity. For single-top quark and J/ψ methods, this assumption is probably conservative, because trigger and selection efficiencies will benefit from the extended coverage of the upgraded detector more than the other $t\bar{t}$ enriched samples. The upgrade of the tracker, calorimeter and muon spectrometer is expected to ensure an efficient reconstruction up to $|\eta|$ about 4 [3].

With respect to Ref. [9], most assumptions regarding expected improvements in the understanding of systematic uncertainties remain unchanged. The modeling of color reconnection

and fragmentation in $t\bar{t}$ events were investigated for the 8 TeV analysis, while underlying event modeling has been studied at both 8 TeV and 13 TeV [19–21]. These studies were partially statistically limited and will benefit from the expected large data samples (abridged by "improved with data" in Table 1–4). This will provide better constraints on the modeling of QCD and fragmentation effects. The use of next-to-leading order (NLO) matrix-element (ME) generators has been established already for the data taking at 13 TeV. Different setups and generators are compared to differential cross section measurements at 8 TeV [22] and parton-shower tunes are being refined. For instance, a tuned value of the α_s and h_{damp} parameters obtained with the data recorded in 2015 will be used in future MC simulations [23]. These parameters take part in the simulation of initial-state radiations and the regulation of the high-p_{T} radiation, respectively. The modeling of the top quark p_{T} in $t\bar{t}$ production by the generators used in the 7 and 8 TeV analyses (Run-1) does not describe the distribution observed in data [24]. As a consequence, a systematic uncertainty was assigned that covered the full difference between observed and simulated top quark p_{T} spectrum. Already with the statistics from Run-1, it was possible to constrain this variation by roughly a factor of 3 [12, 24]. In addition, differential predictions for $t\bar{t}$ production at NNLO are now available [25]. These can be used to provide differential k-factors for the MC simulation which will lead to an additional reduction of the top quark p_{T} uncertainty roughly by a factor of 2. These two points are referred-to as "improved with data" and "NNLO k-factors" in Table 1–4.

The parton density functions (PDF), as well as the b tagging efficiencies are also expected to be more precisely determined with the larger data set expected in the next runs of the LHC (also abridged by "improved with data" in Table 1–4).

To accompany the increase of the data set size, the MC samples generated are assumed to be correspondingly increased in size (labeled "MC stat." in Table 1–4).

For the measurements, certain uncertainties are derived from MC samples generated with different generator configurations. If the resulting variation in m_{t} is below the statistical precision of the MC sample, the uncertainty is traditionally decomposed in two parts: one corresponding to the top quark mass variation, the other one to the statistical precision. For the projections, they are treated separately, before being recombined. The evolution of the first one relies on theoretical developments, while the second one will be likely reduced with the production of larger MC samples ("MC stat."). In some cases, only upper bounds could be determined at 8 TeV and projections are made on their evolution upon all the aforementioned assumptions.

2.2 The reference method in the lepton+jets channel

This technique relies on the full kinematic reconstruction of lepton+jets $t\bar{t}$ candidate events, with m_{t} being inferred from the invariant mass of the top quark decay products simultaneously with a global jet energy scale factor. With 19.7 fb^{-1} of data at 8 TeV, the result obtained is 172.35 ± 0.16 (stat) ± 0.48 (syst) GeV [10], corresponding to a precision better than 0.3%. Events are required to have exactly 1 isolated electron or muon with $p_{\mathrm{T}} > 33$ GeV and $|\eta| < 2.1$ and at least 4 jets with $p_{\mathrm{T}} > 30$ GeV and $|\eta| < 2.4$, amongst which exactly 2 have to be b-tagged.

The main sources of uncertainty are related to the flavor-dependent JES, the branching fractions of semileptonic b hadron decays, the global JES, and the choice of ME generator. The flavor-dependent JES and branching fractions of sempileptonic b hadron decays, together with the b-fragmentation, are the three ways for hadronization modeling to affect this method. Several other aspects of the modeling of perturbative and non-pertubative QCD, such as underlying event modeling or the threshold used for the matching between the tree-level ME generator and the parton showering (PS), also contribute significantly to the systematic uncertainty of

this technique.

The arguments of Ref. [9] are used to predict the values of the uncertainties expected at 14 TeV from those at 8 TeV without new simulations. The results are shown in Table 1, where all of the uncertainties have been conservatively symmetrized. As the cross section for $\mathrm{t\bar{t}}$ production increases more rapidly from 8 TeV to 14 TeV than those of the main background processes (single top quark and W+jets), the uncertainty due to the background modeling is expected to decrease by a factor 3 (shorten to "cross sections" in Table 1). For the uncertainty stemming from the choice of ME generator, the top quark mass measured with a LO ME generator (e.g. MadGraph) is compared to that obained with an NLO generator (e.g. Powheg) at 8 TeV. With the generalized use of NLO ME generators in the future, this category of systematic uncertainty is no longer needed. Also the matching between ME generator and PS is affected. First studies imply a promising reduction of the corresponding uncertainty [26]. However, for the projections presented here, no reduction is assumed.

With 3 ab^{-1} of data, the predicted total uncertainty is less than 0.14 GeV, with a statistical contribution of 0.02 GeV. The underlying event and hadronization modeling uncertainties are expected to be dominant at 14 TeV, though highly reduced by the 3D fit technique, residual energy corrections for b jets, and the foreseen improvements in $\mathrm{t\bar{t}}$ modeling.

Table 1: Summary of the systematic uncertainties on m_{t} for the reference measurement in lepton+jets channel. Experimental uncertainties are separated from theoretical ones.

Source	Value (GeV) 8 TeV, 19.7 fb^{-1}	14 TeV, 0.3 ab^{-1}	14 TeV 3 ab^{-1}	Comment
Method calibration	±0.04	±0.02	±0.02	MC stat. $\times4$
Lepton energy scale	$+0.01$	±0.01	±0.01	unchanged
Global JES	±0.13	±0.12	±0.04	3D fit, differential
Flavor-dependent JES	±0.19	±0.17	±0.06	3D fit, differential
Jet energy resolution	-0.03	±0.02	< 0.01	differential
$E_{\mathrm{T}}^{\mathrm{miss}}$ scale	$+0.04$	±0.04	±0.04	unchanged
b tagging efficiency	$+0.06$	±0.03	±0.03	improved with data
Pileup	-0.04	±0.04	±0.04	unchanged
Backgrounds	$+0.03$	±0.01	±0.01	cross sections
ME generator	-0.12 ± 0.08	–	–	NLO ME generator
Ren. and fact. scales	-0.09 ± 0.07	±0.06	±0.06	NLO ME generator, MC stat.
ME-PS matching	$+0.03 \pm 0.07$	±0.06	±0.06	MC stat.
Top quark p_{T}	$+0.02$	< 0.01	< 0.01	improved with data
b fragmentation	< 0.01	< 0.01	< 0.01	unchanged
Semileptonic b hadron decays	-0.16	±0.11	±0.06	improved with data
Underlying event	$+0.08 \pm 0.11$	±0.14	±0.09	improved with data, MC stat.
Color reconnection	$+0.01 \pm 0.09$	±0.05	< 0.01	improved with data
PDF	±0.04	±0.03	±0.02	improved with data
Systematic uncertainty	±0.48	±0.30	±0.17	
Statistical uncertainty	±0.16	±0.04	±0.02	
Total	±0.51	±0.31	±0.17	

2.3 Top quark mass from single-top quark events

Similar to the measurement of m_t in semileptonic $t\bar{t}$ decays, the top quark is fully reconstructed and m_t is inferred from the invariant mass of all top quark decay products, with the neutrino p_T being retrieved from the momentum imbalance (E_T^{miss}) of the event. The most important difference relative to the method described in Section 2.2 is the contribution of physics processes in the selected sample. A sample enriched with single-top quarks can be obtained by requiring the presence of a forward light jet [27]. The selection efficiency should thus be more sensitive to the extended coverage of the upgraded tracker, calorimeter, and muon spectrometer.

The production of single-top quarks is mediated through electroweak interactions whereas $t\bar{t}$ production occurs through QCD interactions. Thus, the uncertainties related to color reconnection modeling, hard process simulation, and parton distribution functions are quite different. This aspect can provide insights into these modeling effects.

The measurement performed at 8 TeV yields a result of $172.60 \pm 0.77\,(\text{stat})\,^{+0.97}_{-0.93}\,(\text{syst})$ GeV, where the precision is limited by the global and flavor-dependent JES uncertainties. With higher statistics, this uncertainty and others could be reduced by using a similar technique as in lepton+jets $t\bar{t}$ events or by applying the constraints on the JES obtained there to single-top quark events.

Together with the different sensitivity to theoretical uncertainties, an improved extraction of m_t from single-top quark events may contribute significantly to a combination with the m_t results in lepton+jets $t\bar{t}$ events.

The third largest source of systematic uncertainty at 8 TeV is the modeling of the background processes. The corresponding effect of this is expected to decrease at 14 TeV as the $t\bar{t}$ and single top quark production cross sections increase more than the W+jets one ("cross sections"). The projections for the systematic uncertainties with smaller contributions use the same assumptions as previously mentioned. Table 2 summarizes how these uncertainties evolve with increasing integrated luminosity. The global and flavor-dependent JES uncertainties are expected to remain the main contributions to the total uncertainty on m_t. The precision expected for 3 ab^{-1} of data at 14 TeV is below 0.3%, with a systematic uncertainty of 0.45 GeV.

2.4 The "secondary vertex" method

Instead of the jets from the decaying top quarks, the properties of secondary vertices (SV) can be used to construct a m_t-sensitive observable. This method reduces the impact of JES and jet energy resolution uncertainties on the measured m_t. For instance, the b jet reconstruction can be replaced by the b hadron vertex reconstruction, which makes use of charged particles only. The secondary vertex can be combined with the isolated lepton from the W boson decay and m_t can then be inferred from the invariant mass of the combination ($m_{sv\ell}$).

At 8 TeV, this technique suffers from a systematic uncertainty of $^{+1.58}_{-0.97}$ GeV, mostly due to b hadronization modeling [28]. At the timescale of the HL-LHC and with dedicated measurements such as the ones included in Ref. [28], it can be realistically assumed that the b hadronization modeling will be improved. Even though a reduction of the corresponding uncertainties is expected, they still remain a dominant source of systematic uncertainty for this method, as shown in Table 3. Also the contribution from the top quark p_T modeling remains non negligible despite the use of a Lorentz invariant observable. The secondary vertex mass modeling is expected to be improved with more accurate tracking efficiencies and decay tables (referred-to as "upgraded tracker and decay tables" in Table 3).

Table 2: Summary of the systematic uncertainties on m_t for the measurements in the single-top quark t-channel. Experimental uncertainties are separated from theoretical ones.

Source	Value (GeV) 8 TeV, 19.7 fb^{-1}	14 TeV, 0.3 ab^{-1}	14 TeV 3 ab^{-1}	Comment
Fit Calibration	± 0.38	± 0.15	± 0.15	MC stat. $\times 4$, improved method
Lepton energy scale	< 0.05	< 0.05	< 0.05	unchanged
Global JES	$+0.55, -0.46$	± 0.35	± 0.23	benefits from lepton+jets
Flavor-dependent JES	± 0.40	± 0.28	± 0.19	benefits from lepton+jets
Jet energy resolution	< 0.05	< 0.04	< 0.03	benefits from lepton+jets
E_T^{miss}	± 0.15	± 0.15	± 0.15	unchanged
b tagging efficiency	± 0.10	± 0.08	± 0.05	improved with data
Pileup	± 0.10	± 0.10	± 0.10	unchanged
Backgrounds	± 0.39	± 0.20	± 0.20	cross sections
ME generator	± 0.10	–	–	NLO ME generator
Ren. and fact. scales	± 0.23	± 0.07	± 0.07	MC stat.
b quark hadronization	± 0.14	± 0.10	± 0.06	improved with data
Underlying event	± 0.20	± 0.15	± 0.10	improved with data
Color reconnection	< 0.05	< 0.04	< 0.02	improved with data
PDF	< 0.05	< 0.04	< 0.02	improved with data
Systematic uncertainty	$+0.97, -0.93$	± 0.59	± 0.45	
Statistical uncertainty	± 0.77	± 0.20	± 0.06	
Total	$+1.24, -1.21$	± 0.62	± 0.45	

Projections for 3 ab^{-1} at 14 TeV of all uncertainties lead to an expected total uncertainty of ± 0.62 GeV, with a statistical uncertainty of only 0.02 GeV, thus similar to the reference method.

2.5 The "J/ψ " method

Similar to the reconstruction of secondary vertices from charged tracks, this technique makes use of a partial reconstruction of top quarks in leptonic final states containing $J/\psi \to \mu^+\mu^-$ from the b quark fragmentation. The top quark mass is determined through its correlation with the mass of the $J/\psi + \ell$ system ($m_{J/\psi+\ell}$), where ℓ is either a muon or an electron produced in the leptonic decay of the accompanying W boson.

The presence of three leptons in the final state, two of which originate from the J/ψ meson decay, provides a nearly background-free sample of events. It also has the advantage of a reduced dependence on systematic uncertainties linked to initial- and final-state radiation, jet reconstruction and b tagging techniques.

The measurement performed at 8 TeV is statistically limited because of the very small branching fraction of the decay channel of interest [29]. Compared to the secondary vertex method, the systematic uncertainty is smaller, due to the fact that the analysis relies only on the leptons and a smaller sensitivity to fragmentation modeling.

The number of top quark candidates with a $J/\psi \to \mu^+\mu^-$ decay reconstructed with 19.7 fb^{-1} at 8 TeV predicts an event rate of about 1 100 events/10 fb^{-1} at 14 TeV. Scaling the statistical uncertainty with luminosity only results in expected statistical uncertainty on the measured top mass of about 0.24 GeV. As this technique heavily relies on the reconstruction of $J/\psi \to \mu^+\mu^-$,

Table 3: Summary of the systematic uncertainties on m_{t} for the measurement from $m_{\mathrm{sv}\ell}$. Experimental uncertainties are separated from theoretical ones.

Source	Value (GeV) 8 TeV, 19.7 fb^{-1}	14 TeV, 0.3 ab^{-1}	14 TeV 3 ab^{-1}	Comment
Lepton energy scale	$+0.22, -0.26$	±0.26	±0.26	unchanged
Sec. vertex track multiplicity	-0.06	±0.06	±0.06	unchanged
Sec. vertex mass modeling	-0.29	±0.22	±0.15	upgraded tracker and decay tables
Jet energy scale	$+0.19, -0.17$	±0.14	±0.10	benefits from lepton+jets
Jet energy resolution	±0.05	±0.05	±0.05	unchanged
Unclustered energy	$+0.07$	±0.07	±0.07	unchanged
b tagging efficiency	-0.02	±0.02	±0.01	improved with data
Pileup	$+0.07, -0.05$	±0.07	±0.07	unchanged
Lepton selection efficiency	$+0.01$	±0.01	±0.01	unchanged
Backgrounds	< 0.03	±0.01	±0.01	cross sections
$\sigma(\mathrm{t\bar{t}} + \text{heavy flavor})$	$+0.46, -0.36$	±0.33	±0.20	improved with data
ME generator	-0.42	–	–	NLO ME generator
Single t fraction	±0.07	±0.06	±0.06	cross sections
Single t diagram interference	$+0.24$	±0.06	< 0.01	NLO ME generator
Ren. and fact. scales	$+0.30, -0.20$	±0.10	±0.10	NLO ME generator
ME-PS matching	$+0.06, -0.04$	±0.06	±0.06	unchanged
Top quark p_{T}	$+0.82$	±0.14	±0.14	improved with data and NNLO k-factors
Top quark decay width	-0.05	±0.04	±0.02	improved with data
b quark fragmentation	$+1.00, -0.54$	±0.70	±0.40	improved with data
Semileptonic B decays	±0.16	±0.11	±0.06	improved with data
b hadron composition	-0.09	±0.07	±0.04	improved with data
Underlying event	$+0.19$	±0.15	±0.10	improved with data
Color reconnection	$+0.08$	±0.05	±0.02	improved with data
PDF	$+0.06, -0.04$	±0.04	±0.02	improved with data
Systematic uncertainty	$+1.58, -0.97$	±0.95	±0.62	
Statistical uncertainty	±0.20	±0.05	±0.02	
Total	$+1.59, -0.99$	±0.95	±0.62	

the extension of the muon chamber and tracker coverage will contribute to a further decrease of the statistical uncertainty, which is not accounted for here.

Projections of the systematic uncertainties are presented in Table 4. The numbers measured in Ref. [29] are used as a baseline. The relative reduction of these uncertainties follows the assumptions from the previous sections. In addition, the implementation of a constrained J/ψ vertex fit could result in a significant decrease of the uncertainty stemming from the modeling of the J/ψ mass spectrum. The experimental uncertainty is expected to be ultimately less than 0.17 GeV and the theoretical uncertainty around 0.52 GeV. With more constraints on the $\mathrm{t\bar{t}}$ modeling from data, the dominant sources of systematic uncertainties should be the ME-PS matching and top quark p_{T} modeling.

Table 4: Summary of the systematic uncertainties on m_t for the measurement from $m_{J/\psi+\ell}$. Experimental uncertainties are separated from theoretical ones.

Source	Value (GeV) 8 TeV, $19.7\,fb^{-1}$	14 TeV, $0.3\,ab^{-1}$	14 TeV $3\,ab^{-1}$	Comment
Size of the simulation samples	±0.22	±0.07	±0.07	MC stat. $\times10$
Muon momentum scale	±0.09	±0.09	±0.09	unchanged
Electron momentum scale	±0.11	±0.11	±0.11	unchanged
Modeling of $m_{J/\psi}$	$+0.09$	< 0.01	< 0.01	constrained J/ψ vertex fit
Jet energy scale	< 0.01	< 0.01	< 0.01	unchanged
Jet energy resolution	< 0.01	< 0.01	< 0.01	unchanged
Trigger efficiencies	±0.02	±0.01	±0.01	improved method
Pileup	±0.07	±0.07	±0.07	unchanged
Backgrounds	±0.01	±0.01	±0.01	unchanged
ME generator	-0.37	–	–	NLO ME generator
Ren. and fact. scales	$+0.12, -0.46$	±0.08	±0.04	NLO ME generator, MC stat.
ME-PS matching	$+0.12, -0.58$	±0.50	±0.43	MC stat.
Top quark p_T	$+0.64$	±0.12	±0.12	improved with data and NNLO k-factors
b quark hadronization	±0.30	±0.21	±0.12	improved with data
Underlying event	±0.13	±0.10	±0.07	improved with data
Color reconnection	$+0.12$	±0.09	±0.06	improved with data
PDF	$+0.39, -0.11$	±0.27	±0.15	improved with data
Systematic uncertainty	$+0.89, -0.94$	±0.66	±0.53	
Statistical uncertainty	±3.0	±0.77	±0.24	
Total	$+3.13, -3.14$	±1.00	±0.58	

2.6 Top quark pole mass from the $t\bar{t}$ cross section

The techniques presented above are based on the calibration of a m_t-sensitive oberservable using a MC mass calibration. The theoretical interpretation of the results is currently under study [30]. Theoretical predictions beyond next-to-leading order for $t\bar{t}$ production cross section ($\sigma_{t\bar{t}}$) are available with a well-defined scheme for mass renormalization. By comparing these predictions to measurements of $\sigma_{t\bar{t}}$, m_t can be extracted in the same scheme. This technique has been used within the CMS Collaboration at 7 and 8 TeV [12] and at 13 TeV with the first Run-2 data [31].

Table 5 presents the uncertainty sources associated to this measurement at $\sqrt{s} = 7, 8$ and 13 TeV, as well as projections to $\sqrt{s} = 14$ TeV. The uncertainties in the theoretical prediction decrease with $\sqrt{s}$. For the extraction of m_t at $\sqrt{s} = 7$, 8 and 13 TeV, the same PDF sets have been used. With higher centre-of-mass energy, the PDF uncertainty benefits from the production of $t\bar{t}$ pairs at lower gluon momentum fractions, where the PDFs are known with higher precision. The increase in $\sqrt{s}$ is moderate from 13 to 14 TeV, but more constraints on the PDFs and more measurements of $\alpha_S(m_Z)$ are expected. We assume this contribution to the uncertainty on the measured pole mass to decrease by 25% and 50% for $0.3\,ab^{-1}$ and $3\,ab^{-1}$, respectively.

The measured $\sigma_{t\bar{t}}$ receives detector-acceptance corrections which depend on the top quark

mass. These are evaluated using MC simulations. The measured value shows a mildly falling dependence on m_t^{MC} ("Slope"), which leads to a larger uncertainty in the resulting m_t, increasing with $\sqrt{s}$. The uncertainty in m_t increases further from relating this dependence as a function of m_t^{MC} to the prediction as a function of the pole mass (or any other mass in a well-defined scheme). However, it is possible to mitigate the "Slope" effect already with the statistics of the 8 TeV data and in consequence the ambiguity from relating the dependence on the pole mass to the one on m_t^{MC} [32]. This technique is already used for the measurement at 13 TeV. Thus, both contributions are assumed to be negligible for future determinations. The energy of the LHC beams directly affects the predicted cross section and in consequence the extracted top quark mass. For the measurements at 7, 8 and 13 TeV, the beam-energy is assumed to have an uncertainty of about 1.7% [33]. Recent measurements show that this value can be reduced to 0.1% [34], making this uncertainty negligible in the future. In consequence, the dominant contribution to the total uncertainty on m_t is the uncertainty on the measured $t\bar{t}$ cross section. With 0.3 ab^{-1} and 3 ab^{-1}, dedicated techniques which exploit the high statistics for in-situ constraints, similar to the previous measurements, can be employed to significantly reduce the uncertainty on the measurements done in a fiducial phase space. In addition, the extrapolation to the full phase space will have an increased precision if NLO MC and differential predictions at NNLO including the $t\bar{t}$ decay are used. These are assumed to become available. The impact of the uncertainty on the luminosity measurement will become dominant. It is assumed to be reduced to about 1.5% with 3 ab^{-1}. Therefore, it is reasonable to assume a reduction of the total uncertainty from the cross-section measurement by 25% for 0.3 ab^{-1} and 50% for 3 ab^{-1}.

As the result of all improvements, a total uncertainty of about 1.4 GeV for 0.3 ab^{-1} and 1.2 GeV for 3 ab^{-1} on the top quark mass extracted from the $t\bar{t}$ production cross section can be expected.

Table 5: Summary of the systematic uncertainties on m_t for the measurement from $\sigma_{t\bar{t}}$. Experimental uncertainties are separated from theoretical ones.

Source	Value			
	7 & 8 TeV, 25 fb^{-1}	13 TeV, 2.3 fb^{-1}	14 TeV, 0.3 ab^{-1}	14 TeV, 3 ab^{-1}
Predicted $\sigma_{t\bar{t}}$				
PDF and $\alpha_S(m_Z)$ at ME	$\pm$0.5%	$\pm$0.4%	$\pm$0.3%	$\pm$0.2%
Ren. and fact. scales	$\pm$0.6%	$\pm$0.4%	$\pm$0.4%	$\pm$0.4%
Measured $\sigma_{t\bar{t}}$				
Uncertainty	$\pm$0.8%	$\pm$1.3%	$\pm$0.6%	$\pm$0.4%
Slope	$\pm$0.3%	$< 0.1\%$	$< 0.1\%$	$< 0.1\%$
Other uncertainties				
LHC beam energy	$\pm$0.3%	$\pm$0.5%	$< 0.1\%$	$< 0.1\%$
$m_t^{MC} = m_t^{pole}$	$\pm$0.3%	$< 0.1\%$	$< 0.1\%$	$< 0.1\%$
Total uncertainty m_t [%]	$\pm$1.1	$\pm$1.5	$\pm$0.8	$\pm$0.7
Total uncertainty m_t	$\pm$2 GeV	$\pm$2.7 GeV	$\pm$1.4 GeV	$\pm$1.2 GeV

2.7 Conclusions

Figure 1 summarizes the expected precision on m_t for the discussed measurement techniques. The methodology is the same as in Ref. [9] and this Figure supersedes its result. A potential reduction of the trigger efficiency of up to a factor 3 as well as many improvements in the understanding of the systematic uncertainties are expected. With data collected during the Run-1, most analyses were already limited by systematic uncertainties except for the J/ψ method which is still affected by a sizable statistical uncertainty. With 3 ab^{-1} of data, all of the analyses will be limited by systematic uncertainties and especially by theoretical modeling uncertainties. The reference method, which is the most precise one, is expected to yield an ultimate relative precision below 0.1% at HL-LHC. The other techniques, with different systematic sensitivities, are expected to be precise enough to carry significant weight in a combination with the reference method. This would make it possible to further reduce the systematic uncertainties, which are related mostly to the JES and hard process modeling.

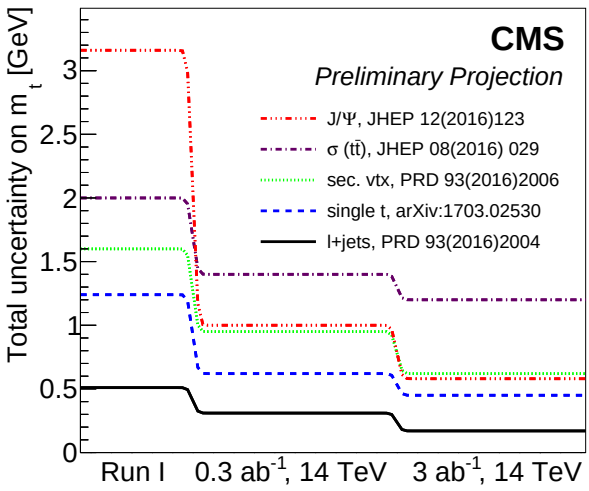

Figure 1: Total uncertainty on top quark mass (m_t) obtained with different measurement methods and their projections to the HL-LHC for running conditions foreseen after the phase II upgrade. The projections for $\sqrt{s} = 14$ TeV, with 0.3 ab^{-1} or 3 ab^{-1} of data, are based on m_t measurements performed at the LHC Run-1, assuming that an upgraded detector will maintain the same physics performance despite a severe pileup.

3 Increase of sensitivity on the search for top quark FCNC

Evidence for physics beyond the SM can be found in measurements of the branching fractions of FCNC in the top quark decays. Top quark FCNC transitions occur at loop level within the SM and are highly suppressed by the Glashow-Iliopoulos-Maiani (GIM) mechanism [35]. The predicted branching fractions for the $t\to u+\gamma$ and $t\to c+\gamma$ decays are approximately 10^{-16} and 10^{-14}, respectively [36]. However, in some extensions of the SM the GIM suppression can be relaxed leading to an enhancement of several orders of magnitude in branching fractions that could be observed at the LHC [37, 38]. As a result, a possible observation of these rare top quark decay modes would provide a clear signature of physics beyond the SM.

Searches for FCNC in top quark decays have been performed in the previous collider experiments and no indications of FCNC $t\to u+\gamma$ and $t\to c+\gamma$ transitions were found. The experiments at LEP and HERA have established upper limits at 95% confidence level (CL) using single-top quark production. The measured limits are 4.1% (L3) [39], 0.64% (H1) [40] and 0.29% (ZEUS) [41], respectively. The CDF experiment at the Tevatron obtained a 95% CL limit of 3.2% on $B(t\to q+\gamma)$ [42] from $t\bar{t}$ production. At the LHC a measurement of the diphoton mass spectrum resulted in an upper limit of $B(t\to q+\gamma) < 0.48\%$ at 95% CL [43]. The most stringent constraints on the $B(t\to q+\gamma)$ are set by the CMS experiment through single-top quark production in association with a photon. The upper 95% CL limit on the branching fractions are $B(t\to u+\gamma) < 0.016\%$ and $B(t\to c+\gamma) < 0.182\%$ [44].

In this Section, the sensitivity of the upgraded CMS detector to $t\to q\gamma$ FCNC transitions is estimated for integrated luminosities of 300 and 3000 fb^{-1}. The search for the FCNC interaction $tq\gamma$ is performed by combining the single-top quark and $t\bar{t}$ production channels. The single-top quark production due to FCNC contains a top quark in association with a photon with no extra jets from the matrix element calculation. In the FCNC signal events from $t\bar{t}$ production, the $tq\gamma$ FCNC coupling appears in the decay of one of the top quarks leading to the same signature as for a single-top quark in association with a photon with an additional up or charm jet in the final state. We focus on the SM decays of the top quark, i.e. top quark decays into a W boson and a bottom quark, followed by the decay of the W boson to a muon and a neutrino.

3.1 Simulation

The simulated samples for both single-top quark in association with a photon ($t\gamma$) and $t\bar{t}$ production with one of the top quark decaying via FCNC ($t\gamma j$) are generated with the MADGRAPH (v. 5.1.5.11) [45] generator interfaced with PYTHIA (v. 6.426) [46] for parton showering and hadronization. The NNPDF23 [47] PDFs are used for modeling the proton PDFs for the LO generators and the top quark mass is set to 172.5 GeV.

The SM background processes are simulated using the techniques developed in Refs. [48, 49] for the common Snowmass SM background processes for future hadron colliders studies. The events are generated using MADGRAPH at parton level interfaced with PYTHIA. A fast simulation of the CMS detector, including pileup effects, is performed with DELPHES3 [50]. During the event processing, datasets are produced considering an average of 200 additional pileup interactions per bunch crossing.

3.2 Event selection

The general characteristics of signal events are the presence of an isolated energetic photon, a muon, large missing transverse momentum and a b jet. The selection of events in this analysis is similar to that used in the FCNC search at 8 TeV [44]. Events are selected requiring the

presence of exactly one muon that passes high purity identification requirements and has $p_{\mathrm{T}} > 25\,\mathrm{GeV}$ and $|\eta| < 2.1$. The event is rejected if it has additional muon candidates or any electron candidates with $p_T > 10\,\mathrm{GeV}$, $|\eta| < 2.5$.

Jets are reconstructed using the anti-k_{T} algorithm with a distance parameter of R = 0.4, $p_{\mathrm{T}} > 30\,\mathrm{GeV}$ and $|\eta| < 2.5$. The event is required to have exactly one jet that passes a b tagging criteria at which the b tagging efficiency is about 70% and the misidentification probability is 18% for c jets, and 1.5% for other jets [51].

Photon candidates are required to be well-identified and to have $p_{\mathrm{T}} > 50\,\mathrm{GeV}$ and $|\eta| < 2.5$ and a relative isolation less than 0.1. The photon candidate is required to be separated from the muon and b-jet directions by $\Delta R(\mu, \gamma) > 0.7$ and $\Delta R(b, \gamma) > 0.7$.

The neutrino from the W decay originating from the top quark is not detected and produces $E_{\mathrm{T}}^{\mathrm{miss}}$ in the detector. The p_{T} of the undetected neutrino is taken to be equal to the magnitude of $E_{\mathrm{T}}^{\mathrm{miss}}$. Events are required to have $E_{\mathrm{T}}^{\mathrm{miss}} > 30\,\mathrm{GeV}$.

In each event, the top quark is reconstructed using the four-momenta of muon, b jet and $E_{\mathrm{T}}^{\mathrm{miss}}$. The longitudinal component of the neutrino momentum is obtained by constraining the invariant mass of the muon candidate and neutrino to the value of the W boson mass. When there are two real solutions for the quadratic equation $m_W^2 = (p_\mu + p_\nu)^2$, the one with the smaller absolute value of the longitudinal component of the neutrino momentum is taken [52]. If there is no real solution, the real part is considered as the z component of the neutrino momentum. By combining the reconstructed W boson and the b jet candidate, the top quark is reconstructed. Finally, only events with a reconstructed top quark mass in the range of 130 to 220 GeV are selected.

The transverse momentum and pseudorapidity distributions of the photon candidates , arising from tuγ FCNC interactions, are presented in Fig. 2. The distributions of various background processes are also depicted. The HL-LHC configuration should allow to extend the η range for the photon candidates reconstruction up to $|\eta| = 4$, the p_{T} distribution of the photon is shown including overflow bins and the $|\eta|$ distribution up to 4.0 are presented in the plots. In the present analysis, the reconstructed photon candidate is required to have similar pseudorapidity cut as the 8 TeV analysis ($|\eta| < 2.5$) as the fake photon background contribution is extrapolated from the results obtained at 8 TeV.

After applying this selection, the main background contributions are coming from tV+jets and VVV+jets, where V includes γ, Z, and $W^{\pm}$. Since DELPHES does not simulate photon misidentification appropriately, the contributions from W+jets, $\mathrm{t\bar{t}}$ and t+jets processes are estimated based on the results from 8 TeV analysis [44]. The contributions of W+jets and $\mathrm{t\bar{t}}$ are found to be 16% and 8% of the total background contribution at 8 TeV. In this analysis, similar constitutions for these backgrounds are assumed. The expected efficiencies of tuγ and tcγ signal processes are found to be 2.30% and 2.34%, respectively. The total number of expected background events is 447898 for an integrated luminosity of 3 ab^{-1}.

3.3 Expected limit

To determine the upper limit on the branching fractions of t→u+γ and t→c+γ, a simple counting method is used. Upper limits are set on the signal cross sections assuming there is no signal contribution in data. The modified frequentist $\mathrm{CL_s}$ approach [53, 54] is used to set the upper limits on potential signal rates using the ROOSTATS package [55].

The total systematic uncertainties on selection efficiencies estimated in the 8 TeV analysis are

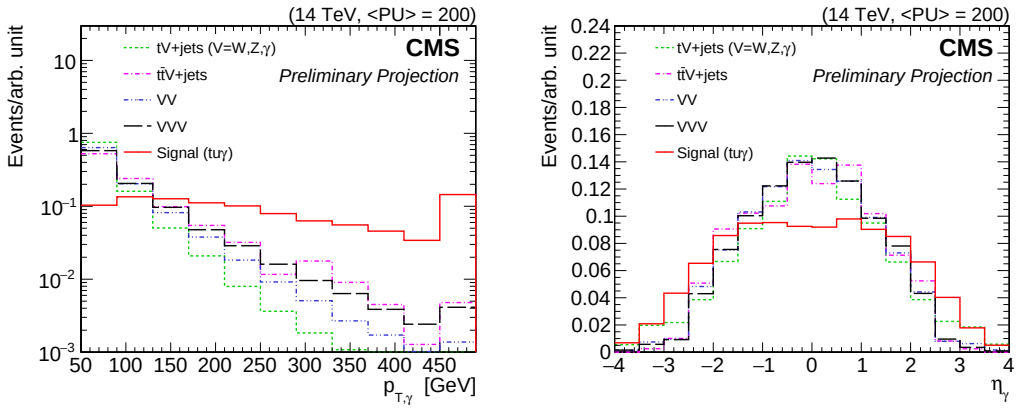

Figure 2: Transverse momentum (left) and pseudorapidity (right) of the photon candidates from t+γ production due to tuγ FCNC interaction and various background processes with V= γ, Z, W. The distributions are obtained using DELPHES simulation for the upgraded CMS detector at $\sqrt{s} = 14$ TeV and on average 200 interactions per bunch crossing.

11.5% and 11.0% for the tuγ and tcγ, respectively. For the tuγ (tcγ), the theoretical uncertainties are contributing to a level of 4.1% (2.8%). For the projection to the HL-LHC, two scenarios for the systematic uncertainties are considered. In scenario 1, the total uncertainty is left unchanged with respect to the 8 TeV analysis, assigning 11.5% and 11.0% for the tuγ and tcγ, respectively. In scenario 2, the theoretical uncertainties are reduced by 50% to 2.05% (1.4%) for the tuγ (tcγ). The experimental uncertainties are assumed to improve with the upgraded detector as follows: the uncertainty in the b tagging efficiency is taken as 1% for b jets, 2% for c jets and 2% for the misidentification of light jets. Lepton isolation and identification efficiencies are assumed to be known with 1% precision, as well as the JES. This uncertainty is propagated to the $E_{\mathrm{T}}^{\mathrm{miss}}$. The uncertainty in the luminosity determination is assumed to be 1.5%. Each uncertainty source is varied individual and the effect is propagated to the final result of the analysis.

The expected upper limits at 95% CL on the branching fractions B(t$\to$u+γ) and B(t$\to$c+γ) for $\sqrt{s} = 14$ TeV with an integrated luminosity of 3 ab^{-1} are shown in Table 6. Limits are presented for scenario 1 and scenario 2. For comparison, the results obtained using 8 TeV data, which correspond to an integrated luminosity of 19.7 fb^{-1}, are shown as well.

Table 6: Upper limits at 95% CL for B(t$\to$u+γ) and B(t$\to$c+γ), obtained with the 8 TeV data and the projections for 14 TeV with an integrated luminosity of 3 ab^{-1} using CMS DELPHES simulation for two scenarios presented in the text.

	19.7 fb^{-1} at 8 TeV	3 ab^{-1} at 14 TeV (Scenario 1)	3 ab^{-1} at 14 TeV (Scenario 2)
B(t$\to$u+γ)	1.7×10^{-4}	4.6×10^{-5}	2.7×10^{-5}
B(t$\to$c+γ)	2.2×10^{-3}	3.4×10^{-4}	2.0×10^{-4}

The 95% CL upper limits on the branching fractions of t$\to$u+γ and t$\to$c+γ are presented for an integrated luminosity up to 3 ab^{-1} in Fig. 3. The black curve is the expected upper limit at 95% CL and green and yellow bands show the ± 1 and ± 2 standard deviations from the expected limits. The results are obtained for scenario 2 where a better understanding of theoretical predictions and an improved detector performance are assumed. The remaining uncertainty has a

large contribution from statistical fluctuations of the MC simulation and is expected to improve significantly with larger MC samples.

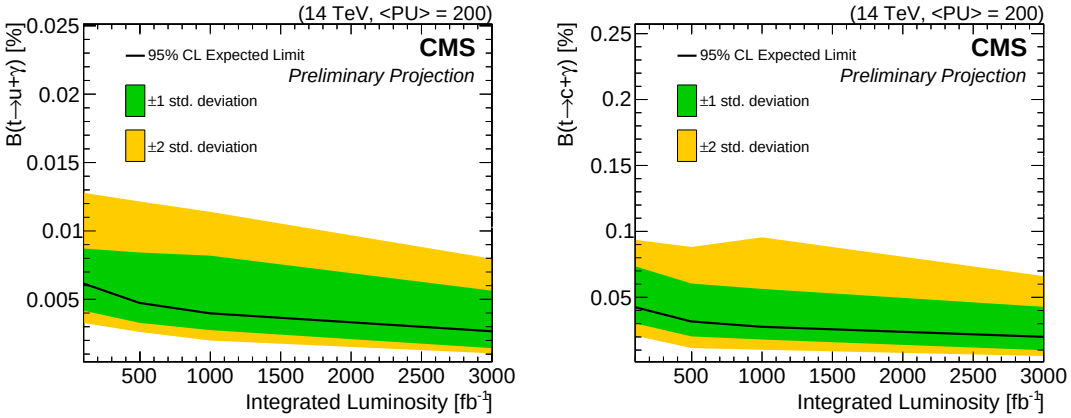

Figure 3: Upper limits at 95% CL on the branching fractions of t→u+γ (left) and t →c+γ (right) for an integrated luminosity up to 3 ab^{-1} at $\sqrt{s}$ = 14 TeV with 200 interactions per bunch crossing on average. The black curve is the expected upper limit at 95% CL and green and yellow bands show the $\pm$1 and $\pm$2 standard deviations from the expected limits. The results are obtained for the scenario 2 that is described in the text.

3.4 Conclusions

Projections for a search for FCNC in top quark production associated with a photon at the HL-LHC are presented. The results are given for pp collisions at $\sqrt{s}$ = 14 TeV, corresponding to an integrated luminosity of 3 ab^{-1}. The upper limits at 95% CL on the branching fractions are B(t→u+γ) < 0.0027% and B(t→c+γ) < 0.020%. Figure 4 shows the expected 95% CL upper limits on B(t→q+Z) and B(t→q+γ) obtained from preliminary projections based on a DELPHES simulation. The horizontal dashed line corresponds to the upper limit on B(t→q+Z) at 14 TeV with 3 ab^{-1} [56]. The two vertical dashed and dashed-dotted lines show the results of this analysis. The two vertical solid lines are the observed CMS results on B(t→u+γ) and B(t→c+γ) at 95% CL [44] and the two solid horizontal lines are the current observed 95% CL upper limits on B(t→u+Z) and B(t→c+Z) from 8 TeV CMS data [57].

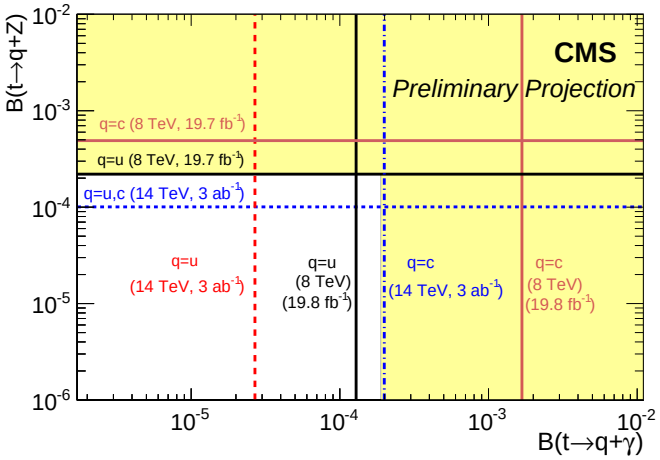

Figure 4: Expected upper limits at 95% CL on B(t→q+Z) and B(t→q+γ) obtained from preliminary projections based on a DELPHES simulation. The horizontal dashed line corresponds to upper limit on B(t→q+Z) at 14 TeV with 3 ab^{-1} [56]. The two vertical dashed and dashed-dotted lines show the results of this analysis. The two vertical solid lines are the observed CMS results on B(t→u+γ) and B(t→c+γ) at 95% CL [44] and the two solid horizontal lines are the current observed 95% CL upper limits on B(t→u+Z) and B(t→c+Z) from 8 TeV CMS data [57].

4 Expected track–trigger performance for the selection of the $B_s^0 \to \phi\phi \to 4K$ events

The $B_s^0 \to \phi\phi \to 4K$ decay is a FCNC process that is forbidden at tree level in the SM. It proceeds predominantly via a $b \to s\bar{s}s$ penguin diagram as shown in Fig. 5. This particularly interesting process can receive contributions in the loop from particles with high masses beyond the LHC energies and can therefore be used to probe new physics at the LHC at energy scales that are not reachable in direct measurements.

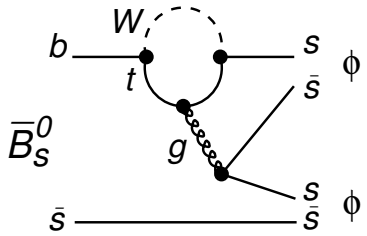

Figure 5: Feynman graph of the dominant amplitude contributing to the decay $B_s^0 \to \phi\phi$.

The transition between quarks is described in the SM by the CKM matrix [58, 59]. The diagonal elements of the matrix are close to one, while off-diagonal ones are very small, thus favoring the charge transition within one quark generation and suppressing transitions between generations. The CP-violation is described by a single phase in the CKM matrix. The SM predictions for the asymmetry in the decay of B_s^0 and $\bar{B}_s^0$ mesons is orders of magnitude smaller than the observed values, therefore measurements of the CP-violating phase ϕ_s plays an important role as probes of SM predictions and in searches for new physics [60]. The phase $\phi_s \simeq 2\beta_s$ is related to the Cabibbo-Kobayashi-Maskawa matrix elements via $\beta_s = \arg(V_{ts}V_{tb}/V_{cs}V_{cb})$.

Measurements of the CP-violation in B_s^0 decays[1] have initially focused on the decay modes $B_s^0 \to J/\psi\phi$, (with $J/\psi \to \mu^+\mu^-$ and $\phi \to K^+K^-$) and $B_s^0 \to J/\psi f_0$ (with $J/\psi \to \mu^+\mu^-$ and $f_0 \to \pi^+\pi^-$) because of the large branching fractions and clean experimental signature of two muons from the J/ψ mesons [61–65]. The former mode is a pseudo-scalar to vector-vector transition, where the final state is an admixture of different CP eigenstates, depending on the relative angular momentum of the J/ψ and ϕ mesons. A measurement of ϕ_s requires the CP-even and CP-odd contributions to be disentangled with an amplitude analysis of the decay angles of the final state particles. The latter mode is a CP-odd final state (with a small percent-level CP-even contribution) and does not require an amplitude analysis for the ϕ_s measurement. Both decay modes proceed in the SM predominantly via a $b \to c\bar{c}s$ transition. With more data, the analyses of these resonant decays have been extended to $B_s^0 \to J/\psi K^+K^-$ and $B_s^0 \to J/\psi \pi^+\pi^-$ [66–68].

The first evidence of $B_s^0 \to \phi\phi$ ($\phi \to K^+K^-$) decay was obtained by the CDF experiment [69] at the Tevatron. It was studied by CDF and LHCb [70–73], who searched for CP-violation in B_s^0 decay time and angular distributions. The LHCb experiment has measured the branching fraction $\mathcal{B}(B_s^0 \to \phi\phi) = (1.84 \pm 0.05\,(\text{stat}) \pm 0.07\,(\text{syst}) \pm 0.11(f_s/f_u) \pm 0.12(\text{norm})) \times 10^{-5}$ [74]. To date, the most precise determination of the phase $\phi_s = -0.17 \pm 0.15\,(\text{stat}) \pm 0.03\,(\text{syst})$ was performed by the LHCb experiment [73], based on a signal sample of approximately 4000 B_s^0 candidates, while the SM QCD factorization calculations provide an upper limit of $\phi_s < 0.02$ [75–77].

The present analysis is a study of the HL-LHC CMS sensitivity for the decay mode $B_s^0 \to \phi\phi$, ($\phi \to K^+K^-$), based on an integrated simulated luminosity of 3000 fb^{-1}. The goal of the analysis is to investigate how well the decay $B_s^0 \to \phi\phi$ can be triggered by the Level1 (L1) system. It should include information from tracking detectors that is currently available only offline. It should be noted that this is the first purely hadronic B decay investigated within the CMS experiment that uses currently only the (di)muon-based analyses [65, 78, 79]. The study of the sensitivity to the ϕ_s measurement is beyond the scope of this analysis.

4.1 Simulation

$B_s^0 \to \phi\phi \to 4K$ signal events have been produced with PYTHIA (v. 6.426) [46] and EvtGen [80] at $\sqrt{s}$ = 14 TeV with kaons having $p_T(K) \geq 2$ GeV. On each signal event on average 140 pileup events have been superimposed. For background, which is predominantly combinatorial in nature, minimum bias events with <PU> = 70, 140, or 200 are used.

4.2 Analysis strategy

The goal of the analysis is to study if $B_s^0 \to \phi\phi \to 4K$ events can be triggered with high efficiency at L1 using only the tracks reconstructed at that level (L1 tracks). The algorithm first reconstructs ϕ candidates from pairs of oppositely charged L1 tracks constrained to come from the same (primary) vertex and then reconstructs B_s^0 candidate(s) from a pair of ϕ candidates. Since the p_T of the lowest-p_T kaon lies very close to the lowest possible trigger threshold of the L1 tracking, there could be loss of signal efficiency. The same analysis is repeated at the offline level with tracks reconstructed with much higher precision to understand if any further reduction of the efficiency will be incurred at the offline analysis level.

4.3 Event selection

To explore different signal selection efficiencies and trigger rates, three different working points for the event selection are defined: loose, medium and tight. The corresponding requirements are listed in Table 7. The distributions of different discriminating variables: the invariant mass

[1] Charge conjugation is implied throughout; exceptions will be obvious.

of the K^+ and the K^- candidate, $M_{K^+K^-}$, the ΔR between the ϕ candidates, $\Delta R(\phi\text{-pair})$, and the invariant mass of the ϕ candidates, $M_{\phi\phi}$ are presented in Figs. 6, 7, 8 for signal events at the trigger and offline reconstruction levels and for background events at the trigger level. It can be noticed that the tail of the signal distributions, both L1 and offline, looks very similar to background because the contribution comes mainly from combinatorics of pileup tracks.

Table 7: Baseline event selection conditions. The variable d_z represents distance between a pair of tracks or trajectories of a pair of reconstructed particles along the beam axis (z) while d_{xy} represents that in the plane perpendicular to the beam axis (xy).

Working point	loose	medium	tight
Tracks	$p_T \geq 2\,\text{GeV}, \lvert\eta\rvert \leq 2.5$		
Track pair	$d_{xy} \leq 1\,\text{cm}, \lvert d_z\rvert \leq 1\,\text{cm}$		$d_{xy} \leq 0.5\,\text{cm}, \lvert d_z\rvert \leq 0.3\,\text{cm}$
ϕ-pair	$d_{xy} \leq 1\,\text{cm}, \lvert d_z\rvert \leq 1\,\text{cm}$		$d_{xy} \leq 0.5\,\text{cm}, \lvert d_z\rvert \leq 1\,\text{cm}$
ϕ-pair	$0.2 \leq \Delta R(\phi_1, \phi_2) \leq 1, \Delta R(K^+, K^-) \leq 0.12$		
ϕ mass	$0.99 \leq M_{K^+K^-} \leq 1.04\,\text{GeV}$		$1.0 \leq M_{K^+K^-} \leq 1.03\,\text{GeV}$
B_s^0 mass	$5.27 \leq M_{\phi\phi} \leq 5.49\,\text{GeV}$		$5.29 \leq M_{\phi\phi} \leq 5.48\,\text{GeV}$

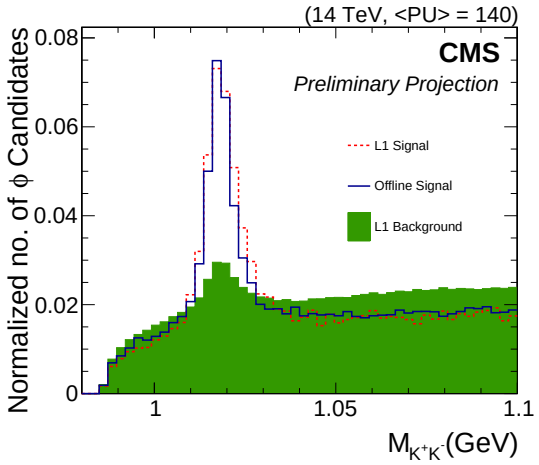

Figure 6: Invariant mass distribution of all track pairs with opposite charges, $|d_z| < 1\,\text{cm}$, $d_{xy} < 1\,\text{cm}$, track $p_T > 2\,\text{GeV}$, and assuming that the tracks are arising from kaons. The event sample does not have a preliminary selection on the B_s^0 mass window. The distributions are normalized to unit area. The blue solid histogram corresponds to the signal events reconstructed with offline tracks, the red dashed one with tracks from L1 trigger system and the green filled area represents the background events.

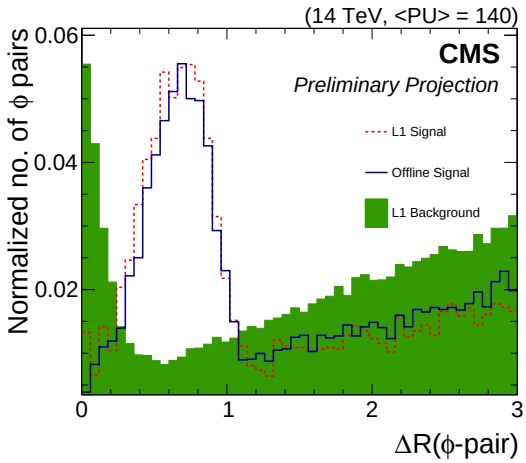

Figure 7: $\Delta R(\phi\text{-pair})$ distribution for all ϕ-pairs with $0.99 < M_{K^+K^-} < 1.04\,\text{GeV}$, $|d_z| < 1\,\text{cm}$, $d_{xy} < 1\,\text{cm}$. The event sample does not have a preliminary selection on the B_s^0 mass window. The distributions are normalized to unit area. The blue solid histogram corresponds to the signal events reconstructed with offline tracks, the red dashed one with tracks from L1 trigger system and the green filled area represents the background events.

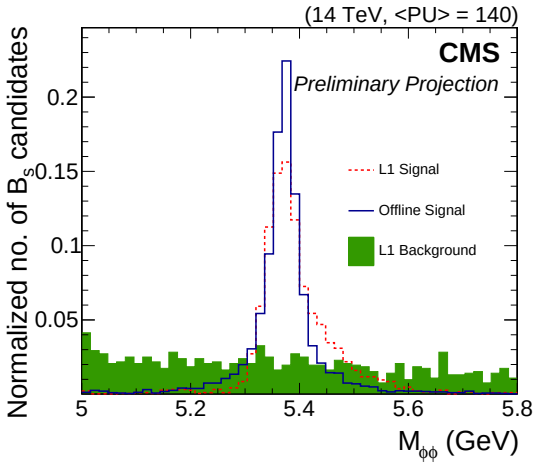

Figure 8: Invariant mass distribution of all the ϕ-pairs with $|d_z|$ (ϕ-pair) $< 1\,\text{cm}$, d_{xy} (ϕ-pair) $< 1\,\text{cm}$, $0.2 < \Delta R$ (ϕ-pair) < 1, $\Delta R(K^+, K^-) < 0.12$. The distributions are normalized to unit area. The blue solid histogram corresponds to the signal events reconstructed with offline tracks, the red dashed one with tracks from L1 trigger system and the green filled area represents the background events.

4.4 Results

Table 8 summarizes the efficiencies and trigger rates for all the three event selection baselines. Here, the efficiency is defined as the fraction of the generated signal events passing all selection requirements. The trigger rate describes the frequency with which signal or background events fulfill the requirements. The rate is given for three different pileup scenarios. The results are also presented in graphical form in Fig. 9. According to the present understanding of the expected detector performance, a rate of about 10 kHz is within the acceptable limit. For the scenario with 200 pileup events this rate can only be sustained for a moderate signal efficiency.

Table 8: Efficiency and rate for loose, medium and tight baselines respectively. Pileup dependence of event rate is also presented for <PU> = 70, 140 and 200. Uncertainties are statistical only.

Baseline	Efficiency (%)		Rate (kHz)		
	L1	Offline	<PU> = 70	<PU> = 140	<PU> = 200
Loose	41.6 ± 1.2	61.5 ± 1.3	6.3 ± 1.5	27.9 ± 1.7	61.8 ± 5.2
Medium	36.6 ± 1.1	55.3 ± 1.2	2.5 ± 0.9	13.3 ± 1.2	29.6 ± 3.6
Tight	31.1 ± 1.0	55.1 ± 1.2	1.4 ± 0.7	5.1 ± 0.7	12.2 ± 2.3

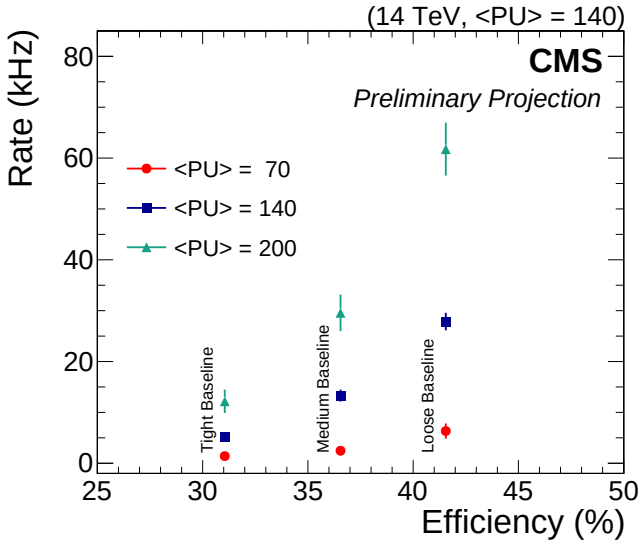

Figure 9: Efficiency and rate for different selection baselines and for different pileup scenarios. Uncertainties are statistical only.

4.5 Conclusions

The $B_s^0 \to \phi\phi \to 4K$ is an important decay channel to investigate the capabilities of the HL-LHC CMS detector in low-p_T fully-hadronic final states. The study is performed with respect to the L1 and offline signal efficiencies and the L1 trigger rate is estimated for several selection and pileup scenarios. The efficiency of the track trigger is expected to be sufficient, while further improvements are required to keep a low trigger rate, e.g. including a displaced vertex finding tool for low-p_T tracks and mitigation of pileup effects.

5 Summary

The three physics proposals for the upgrade studies for the HL-LHC CMS detector discussed in this note were prepared for and presented at the ECFA 2016 workshop.

It is demonstrated that with $3\,\text{ab}^{-1}$ of data the top quark mass analyses will be limited by systematic uncertainties, and especially by theoretical modeling uncertainties. The reference method, which is the most precise one, is expected to yield an ultimate relative precision below 0.1%. The other techniques, with alternative systematic sensitivity, are expected to reach a precision good enough to carry weight in a combination with the reference method. This would make it possible to further reduce the systematic uncertainties, which are related mostly to the JES and hard process modeling.

According to the projections for a search for the FCNC process in the top quark production associated with a photon at a luminosity of 3 ab^{-1} upper limits at 95% CL on the branching fractions B(t$\rightarrow$u+γ) $<$ 0.0027% and B(t$\rightarrow$c+γ) $<$ 0.020% are expected.

The $B_s^0 \rightarrow \phi\phi \rightarrow 4K$ channel is used to investigate capabilities of the HL-LHC CMS detector to trigger events in the low-p_T region for fully-hadronic final states. The study uses the track trigger to estimate the efficiency for selecting the signal events and the trigger rate of the background events. It is demonstrated that with the track trigger sufficient efficiency can be achieved, while the trigger rate requires further improvement e.g. by including displaced vertex finding tool for low p_T tracks and a mitigation of pileup effects.

References

[1] G. Apollinari et al., "High-Luminosity Large Hadron Collider (HL-LHC) : Preliminary Design Report", doi:10.5170/CERN-2015-005.

[2] D. Contardo et al., "Technical Proposal for the Phase-II Upgrade of the CMS Detector", Technical Report CERN-LHCC-2015-010. LHCC-P-008. CMS-TDR-15-02, Geneva, Jun, 2015.

[3] CMS Collaboration, "Technical Proposal for the Phase-II Upgrade of the CMS Detector", Technical Proposal CERN-LHCC-2015-010. LHCC-P-008. CMS-TDR-15-02, CERN, 2015.

[4] "3rd ECFA High Luminosity LHC Workshop", 2016. https://indico.cern.ch/event/524795/.

[5] G. Degrassi et al., "Higgs mass and vacuum stability in the Standard Model at NNLO", *JHEP* **08** (2012) 1, doi:10.1007/JHEP08(2012)098, arXiv:1205.6497.

[6] F. Bezrukov, M. Y. Kalmykov, B. A. Kniehl, and M. Shaposhnikov, "Higgs boson mass and new physics", *JHEP* **10** (2012) 140, doi:10.1007/JHEP10(2012)140, arXiv:1205.2893.

[7] F. Bezrukov and M. Shaposhnikov, "The Standard Model Higgs boson as the inflaton", *Phys. Lett. B* **659** (2008) 703, doi:10.1016/j.physletb.2007.11.072, arXiv:0710.3755.

[8] A. D. Simone, M. P. Herzberg, and F. Wilczek, "Running inflation in the Standard Model", *Phys. Lett. B* **678** (2009) 1, doi:10.1016/j.physletb.2009.05.054, arXiv:0812.4946.

[9] CMS Collaboration, "Projected improvement of the accuracy of top-quark mass measurements at the upgraded LHC", CMS Physics Analysis Summary CMS-PAS-FTR-13-017, CERN, 2013.

[10] CMS Collaboration, "Measurement of the top quark mass using proton-proton data at $\sqrt{s} = 7$ and 8 TeV", *Phys. Rev. D* **93** (2016) 072004, doi:10.1103/PhysRevD.93.072004, arXiv:1509.04044.

[11] A. H. Hoang, "The Top Mass: Interpretation and Theoretical Uncertainties", in *Proceedings, 7th International Workshop on Top Quark Physics (TOP2014): Cannes, France, September 28-October 3, 2014*. 2014. arXiv:1412.3649.

[12] CMS Collaboration, "Measurement of the $\mathrm{t\bar{t}}$ production cross section in the eμ channel in proton-proton collisions at $\sqrt{s} = 7$ and 8 TeV", *JHEP* **08** (2016) 029, doi:10.1007/JHEP08(2016)029, arXiv:1603.02303.

[13] ATLAS Collaboration, "Measurement of the Top Quark Mass from $\sqrt{s} = 7$ TeV ATLAS Data using a 3-dimensional Template Fit", ATLAS Conference Note ATLAS-CONF-2013-046, CERN, 2013.

[14] CMS Collaboration, "Calculation of residual energy correction for b jets using Z+b events in 8 TeV pp Collisions", CMS Physics Analysis Summary CMS-PAS-JME-13-001, CERN, 2014.

[15] CMS Collaboration, "Measurement of the top quark mass in the dileptonic $\mathrm{t\bar{t}}$ decay channel using the $M_{b\ell}$, M_{T2}, and MAOS $M_{b\ell\nu}$ observables", CMS Physics Analysis Summary CMS-PAS-TOP-15-008, CERN, 2016.

[16] CMS Collaboration Collaboration, "Measurement of the top quark mass using proton-proton data at $\sqrt{s} = 7$ and 8 TeV", *Phys. Rev. D* **93** (Sep, 2015) 072004. 56 p. Comments: Submitted to Phys. Rev. D.

[17] CMS Collaboration, "Pileup Removal Algorithms", CMS Physics Analysis Summary CMS-PAS-JME-14-001, CERN, 2014.

[18] M. Czakon, P. Fiedler, and A. Mitov, "Total Top-Quark Pair-Production Cross Section at Hadron Colliders Through $\mathcal{O}(\alpha_S^4)$", *Phys. Rev. Lett.* **110** (2013) 252004, doi:10.1103/PhysRevLett.110.252004, arXiv:1303.6254.

[19] CMS Collaboration, "Study of the underlying event, b-quark fragmentation and hadronization properties in $\mathrm{t\bar{t}}$ events", CMS Physics Analysis Summary CMS-PAS-TOP-13-007, CERN, 2013.

[20] CMS Collaboration, "Measurement of the top quark mass using charged particles in pp collisions at $\sqrt{s} = 8\,\mathrm{TeV}$", *Phys. Rev. D* **93** (2016) 2006, doi:10.1103/PhysRevD.93.092006, arXiv:1603.06536.

[21] CMS Collaboration, "Underlying event measurement with $\mathrm{t\bar{t}}$ +X events with p-p collision data at $\sqrt{s} = 13\,\mathrm{TeV}$", CMS Physics Analysis Summary CMS-PAS-TOP-15-017, CERN, 2015.

[22] CMS Collaboration, "Comparisons of Theory Predictions for the $\mathrm{t\bar{t}}$ Process with Data from pp Collisions at $\sqrt{s} = 8\,\mathrm{TeV}$", CMS Physics Analysis Summary CMS-PAS-TOP-15-011, CERN, 2015.

[23] CMS Collaboration, "Investigations of the impact of the parton shower tuning in Pythia 8 in the modelling of $\mathrm{t\bar{t}}$ at $\sqrt{s} = 8$ and $13\,\mathrm{TeV}$", CMS Physics Analysis Summary CMS-PAS-TOP-16-021, CERN, 2016.

[24] CMS Collaboration, "Measurement of the differential cross section for top quark pair production in pp collisions at $\sqrt{s} = 8\,\mathrm{TeV}$", *Eur. Phys. J. C* **75** (2015) 542, doi:10.1140/epjc/s10052-015-3709-x, arXiv:1505.04480.

[25] M. Czakon, D. Heymes, and A. Mitov, "High-precision differential predictions for top-quark pairs at the LHC", *Phys. Rev. Lett.* **116** (2016) 2003, doi:10.1103/PhysRevLett.116.082003, arXiv:1511.00549.

[26] CMS Collaboration Collaboration, "Measurement of the top quark mass with muon+jets final states in pp collisions at $\sqrt{s} = 13$ TeV", Technical Report CMS-PAS-TOP-16-022, CERN, Geneva, 2017.

[27] CMS Collaboration, "Measurement of the top quark mass from single-top production events", CMS Physics Analysis Summary CMS-PAS-TOP-15-001, CERN, 2016.

[28] CMS Collaboration, "Measurement of the top quark mass using charged particles in pp collisions at $\sqrt{s} = 8$ TeV", *Phys. Rev. D* **93** (2016) 2006, doi:10.1103/PhysRevD.93.092006, arXiv:1603.06536.

[29] CMS Collaboration, "Measurement of the mass of the top quark in decays with a J/ψ meson in pp collisions at 8 TeV", *JHEP* **12** (2016) 123, doi:10.1007/JHEP12(2016)123, arXiv:1608.03560.

[30] M. Butenschoen et al., "Top Quark Mass Calibration for Monte Carlo Event Generators", *Phys. Rev. Lett.* **117** (2016), no. 23, 232001, doi:10.1103/PhysRevLett.117.232001, arXiv:1608.01318.

[31] CMS Collaboration, "Measurement of the $\mathrm{t\bar{t}}$ production cross section using events with one lepton and at least one jet in pp collisions at $\sqrt{s} = 13$ TeV", arXiv:1701.06228.

[32] J. Kieseler, K. Lipka, and S.-O. Moch, "Calibration of the Top-Quark Monte Carlo Mass", *Phys. Rev. Lett.* **116** (2016) 2001, doi:10.1103/PhysRevLett.116.162001, arXiv:1511.00841.

[33] J. Wenninger, "Energy Calibration of the LHC Beams at 4 TeV", Technical Report CERN-ATS-2013-040, CERN, Geneva, 2013.

[34] J. Wenninger and E. Todesco, "Large Hadron Collider momentum calibration and accuracy", Technical Report CERN-ACC-2017-0007, CERN, Geneva, Feb, 2017.

[35] S. L. Glashow, J. Iliopoulos, and L. Maiani, "Weak Interactions with Lepton Hadron Symmetry", *Phys. Rev. D* **2** (1970) 1285, doi:10.1103/PhysRevD.2.1285.

[36] J. A. Aguilar-Saavedra and B. M. Nobre, "Rare top decays $t \to c\gamma, t \to cg$ and CKM unitarity", *Phys. Lett. B* **553** (2003) 251, doi:10.1016/S0370-2693(02)03230-6, arXiv:hep-ph/0210360.

[37] G. Couture, M. Frank, and H. Konig, "Supersymmetric QCD flavor changing top quark decay", *Phys. Rev. D* **56** (1997) 4213, doi:10.1103/PhysRevD.56.4213, arXiv:hep-ph/9704305.

[38] G. R. Lu, F. R. Yin, X. L. Wang, and L. D. Wan, "Rare top quark decays t→cV in the topcolor assisted technicolor model", *Phys. Rev. D* **68** (2003) 015002, doi:10.1103/PhysRevD.68.015002, arXiv:hep-ph/0303122.

[39] L3 Collaboration, "Search for Single Top Production at LEP", *Phys. Lett. B* **549** (2002) 290, doi:10.1016/S0370-2693(02)02933-7, arXiv:hep-ex/0210041.

[40] H1 Collaboration, "Search for Single Top Quark Production at HERA", *Phys. Lett. B* **678** (2009) 450, doi:10.1016/j.physletb.2009.06.057, arXiv:0904.3876.

[41] ZEUS Collaboration, "Search for single-top production in ep collisions at HERA", *Phys. Lett. B* **708** (2012) 27, doi:10.1016/j.physletb.2012.01.025, arXiv:1111.3901.

[42] CDF Collaboration, "Search for Flavor-Changing Neutral Current Decays of the Top Quark in $\mathrm{p\bar{p}}$ Collisions at $\sqrt{s}$ =1.8 TeV", *Phys. Rev. Lett.* **80** (1998) 2525, doi:10.1103/PhysRevLett.80.2525.

[43] S. Khatibi and M. Mohammadi Najafabadi, "Constraints on top quark flavor changing neutral currents using diphoton events at the LHC", *Nucl. Phys. B* **909** (2016) 607, doi:10.1016/j.nuclphysb.2016.06.009, arXiv:1511.00220.

[44] CMS Collaboration, "Search for anomalous single top quark production in association with a photon in pp collisions at $\sqrt{s} = 8$ TeV", *JHEP* **04** (2016) 035, doi:10.1007/JHEP04(2016)035, arXiv:1511.03951.

[45] J. Alwall et al., "The automated computation of tree-level and next-to-leading order differential cross sections, and their matching to parton shower simulations", *JHEP* **07** (2014) 079, doi:10.1007/JHEP07(2014)079, arXiv:1405.0301.

[46] T. Sjöstrand, S. Mrenna, and P. Skands, "PYTHIA 6.4 physics and manual", *JHEP* **05** (2006) 026, doi:10.1088/1126-6708/2006/05/026, arXiv:hep-ph/0603175.

[47] R. D. Ball et al., "Parton distributions with LHC data", *Nucl. Phys.* **B867** (2013) 244–289, doi:10.1016/j.nuclphysb.2012.10.003, arXiv:1207.1303.

[48] A. Avetisyan et al., "Methods and Results for Standard Model Event Generation at $\sqrt{s}$ = 14 TeV, 33 TeV and 100 TeV Proton Colliders (A Snowmass Whitepaper)", arXiv:1308.1636.

[49] J. Anderson et al., "Snowmass Energy Frontier Simulations", arXiv:1309.1057.

[50] J. de Favereau et al., "DELPHES 3, A modular framework for fast simulation of a generic collider experiment", *JHEP* **1402** (2013) 057, doi:10.1007/JHEP02(2014)057, arXiv:1307.6346.

[51] CMS Collaboration, "Performance of the b-jet identification in CMS", *CMS Physics Analysis Summary* **CMS-PAS-BTV-11-001** (2011).

[52] CMS Collaboration, "Measurement of the t-channel single top quark production cross section in pp collisions at $\sqrt{s} = 7$ TeV", *Phys. Rev. Lett.* **107** (2011) 091802, doi:10.1103/PhysRevLett.107.091802.

[53] A. L. Read, "Presentation of search results: the CL_s technique", *J. Phys. G* **28** (2002) 2693, doi:10.1088/0954-3899/28/10/313.

[54] T. Junk, "Confidence level computation for combining searches with small statistics", *Nucl. Instrum. Meth. A* **434** (1999) 435, doi:10.1016/S0168-9002(99)00498-2.

[55] L. Moneta et al., "The RooStats Project", in *13th International Workshop on Advanced Computing and Analysis Techniques in Physics Research (ACAT2010)*. SISSA, 2010. arXiv:1009.1003. PoS(ACAT2010)057.

[56] CMS Collaboration, "Projections for Top FCNC Searches in 3000 fb^{-1} at the LHC", CMS Physics Analysis Summary CMS-PAS-FTR-13-016, CERN, 2013.

[57] CMS Collaboration, "Search for associated production of a Z boson with a single top quark and for tZ flavour-changing interactions in pp collisions at $\sqrt{s} = 8$ TeV", arXiv:1702.01404.

[58] M. Kobayashi and T. Maskawa, "CP Violation in the Renormalizable Theory of Weak Interaction", *Prog. Theor. Phys.* **49** (1973) 652–657, doi:10.1143/PTP.49.652.

[59] N. Cabibbo, "Unitary Symmetry and Leptonic Decays", *Phys. Rev. Lett.* **10** (1963) 531–533, doi:10.1103/PhysRevLett.10.531. [,648(1963)].

[60] J. Charles et al., "Predictions of selected flavour observables within the Standard Model", *Phys. Rev.* **D84** (2011) 033005, doi:10.1103/PhysRevD.84.033005, arXiv:1106.4041.

[61] D0 Collaboration, "Measurement of the CP-violating phase $\phi_s^{J/\psi\phi}$ using the flavor-tagged decay $B_s^0 \to J/\psi\phi$ in 8 fb^{-1} of $p\bar{p}$ collisions", *Phys. Rev.* **D85** (2012) 032006, doi:10.1103/PhysRevD.85.032006, arXiv:1109.3166.

[62] CDF Collaboration, "Measurement of the CP-Violating Phase $\beta_s^{J/\psi\phi}$ in $B_s^0 \to J/\psi\phi$ Decays with the CDF II Detector", *Phys. Rev.* **D85** (2012) 072002, doi:10.1103/PhysRevD.85.072002, arXiv:1112.1726.

[63] LHCb Collaboration, "Measurement of the CP-violating phase ϕ_s in the decay $B_s^0 \to J/\psi\phi$", *Phys. Rev. Lett.* **108** (2012) 101803, doi:10.1103/PhysRevLett.108.101803, arXiv:1112.3183.

[64] ATLAS Collaboration, "Time-dependent angular analysis of the decay $B_s^0 \to J/\psi\phi$ and extraction of $\Delta\Gamma_s$ and the CP-violating weak phase ϕ_s by ATLAS", *JHEP* **12** (2012) 072, doi:10.1007/JHEP12(2012)072, arXiv:1208.0572.

[65] CMS Collaboration, "Measurement of the CP-violating weak phase ϕ_s and the decay width difference $\Delta\Gamma_s$ using the $B_s^0 \to J/\psi\phi(1020)$ decay channel in pp collisions at $\sqrt{s} = 8$ TeV", *Phys. Lett.* **B757** (2016) 97–120, doi:10.1016/j.physletb.2016.03.046, arXiv:1507.07527.

[66] LHCb Collaboration, "Measurement of CP violation and the B_s^0 meson decay width difference with $B_s^0 \to J/\psi K^+K^-$ and $B_s^0 \to J/\psi\pi^+\pi^-$ decays", *Phys. Rev.* **D87** (2013) 2010, doi:10.1103/PhysRevD.87.112010, arXiv:1304.2600.

[67] LHCb Collaboration, "Measurement of the CP-violating phase ϕ_s in $\overline{B}_s^0 \to J/\psi\pi^+\pi^-$ decays", *Phys. Lett. B* **736** (2014) 186–195, doi:10.1016/j.physletb.2014.06.079, arXiv:1405.4140.

[68] LHCb Collaboration, "Precision measurement of CP violation in $B_s^0 \to J/\psi K^+K^-$ decays", *Phys. Rev. Lett.* **114** (2015) 1801, doi:10.1103/PhysRevLett.114.041801, arXiv:1411.3104.

[69] CDF Collaboration, "First evidence for $B_s^0 \to \phi\phi$ decay and measurements of branching ratio and A_{CP} for $B^+ \to \phi K^+$", *Phys. Rev. Lett.* **95** (2005) 031801, doi:10.1103/PhysRevLett.95.031801, arXiv:hep-ex/0502044.

[70] CDF Collaboration, "Measurement of Polarization and Search for CP-Violation in $B_s^0 \to \phi\phi$ Decays", *Phys. Rev. Lett.* **107** (2011) 261802, doi:10.1103/PhysRevLett.107.261802, arXiv:1107.4999.

[71] LHCb Collaboration, "First measurement of the CP-violating phase in $B_s^0 \to \phi\phi$ decays", *Phys. Rev. Lett.* **110** (2013) 1802, doi:10.1103/PhysRevLett.110.241802, arXiv:1303.7125.

[72] LHCb Collaboration, "Measurement of the polarization amplitudes and triple product asymmetries in the $B_s^0 \to \phi\phi$ decay", *Phys. Lett.* **B713** (2012) 369–377, doi:10.1016/j.physletb.2012.06.012, arXiv:1204.2813.

[73] LHCb Collaboration, "Measurement of CP violation in $B_s^0 \to \phi\phi$ decays", *Phys. Rev.* **D90** (2014) 2011, doi:10.1103/PhysRevD.90.052011, arXiv:1407.2222.

[74] LHCb Collaboration, "Measurement of the $B_s^0 \to \phi\phi$ branching fraction and search for the decay $B^0 \to \phi\phi$", *JHEP* **10** (2015) 053, doi:10.1007/JHEP10(2015)053, arXiv:1508.00788.

[75] M. Bartsch, G. Buchalla, and C. Kraus, "$B \to V(L)V(L)$ Decays at Next-to-Leading Order in QCD", arXiv:0810.0249.

[76] M. Beneke, J. Rohrer, and D. Yang, "Branching fractions, polarisation and asymmetries of $B \to VV$ decays", *Nucl. Phys. B* **774** (2007) 64–101, doi:10.1016/j.nuclphysb.2007.03.020, arXiv:hep-ph/0612290.

[77] H.-Y. Cheng and C.-K. Chua, "QCD Factorization for Charmless Hadronic B_s Decays Revisited", *Phys. Rev. D* **80** (2009) 114026, doi:10.1103/PhysRevD.80.114026, arXiv:0910.5237.

[78] CMS Collaboration, "Measurement of the Strange B Meson Production Cross Section with $J/\psi\phi$ Decays in pp Collisions at $\sqrt{s} = 7$ TeV", *Phys. Rev.* **D84** (2011) 052008, doi:10.1103/PhysRevD.84.052008, arXiv:1106.4048.

[79] CMS Collaboration, "Measurement of the $B_s \to \mu^+\mu^-$branching fraction and search for $B^0 \to \mu^+\mu^-$ with the CMS Experiment", *Phys. Rev. Lett.* **111** (2013) 101804, doi:10.1103/PhysRevLett.111.101804, arXiv:1307.5025.

[80] D. J. Lange, "The EvtGen particle decay simulation package", *Nucl. Instrum. Meth.* **A462** (2001) 152–155, doi:10.1016/S0168-9002(01)00089-4.